

Origin of the Dashuigou independent tellurium deposit at Qinghai–Xizang Plateau: constraints from the light stable isotopes C, O, and H

Jianzhao Yin^{1,2} · Yuhong Chao³ · Haoyu Yin⁴ · Hongyun Shi⁵ · Shoupu Xiang⁶

Received: 28 October 2023 / Revised: 28 October 2023 / Accepted: 29 November 2023 / Published online: 11 January 2024
© The Author(s), under exclusive licence to Science Press and Institute of Geochemistry, CAS and Springer-Verlag GmbH Germany, part of Springer Nature 2024

Abstract By studying the light isotopic compositions of carbon, oxygen, and hydrogen, combined with previous research results on the ore-forming source of the deposit, the authors try to uncover its metallogenetic origin. The $\delta^{18}\text{O}$ and $\delta^{13}\text{C}$ isotope signatures of dolomite samples vary between 10.2 and 13.0‰, and between –7.2 and –5.2‰, respectively, implying that the carbon derives from the upper mantle. δD and $\delta^{18}\text{O}$ of quartz, biotite, and muscovite from different ore veins of the deposit vary between –82 and –59‰, and between 11.6 and 12.4‰, respectively, implying that the metallogenetic solutions are mainly magmatic. According to the relevant research results of many isotope geologists, the fractionation degree of hydrogen isotopes increases as the depth to the Earth's core increases, and the

more differentiated the hydrogen isotopes are, the lower their values will be. In other words, mantle-derived solutions can have extremely low hydrogen isotope values. This means that the $\delta\text{D}\text{‰}$ value – 134 of the pyrrhotite sample numbered SD-34 in this article may indicate mantle-derived ore-forming fluid of the deposit. The formation of the Dashuigou tellurium deposit occurred between 91.71 and 80.19 Ma.

Keywords Carbon, oxygen, and hydrogen isotopes · Origin · Independent tellurium deposit · The Qinghai–Xizang Plateau

1 Introduction

The average content of tellurium (Te) in the Earth's crust is 2.0×10^{-9} in China, and 1.34×10^{-9} worldwide (Li 1976). Because of its extremely low Clark value, Te was believed by the traditional geological theory that it could not form independent deposits but only occurred as an associated component in other metallic deposits (Yin et al. 1995d; Yin 1996a; Yin and Shi 2020a).

Many people have never heard of tellurium. However, this is about to change, as a next-generation battery that is smaller and more powerful than presently available will be produced (Cheng et al. 2020). The key material for this kind of battery is tellurium, which has high electrical conductivity and a high volumetric capacity. As a result, tellurium will become more and more popular and well-known in the near future. While rechargeable lithium-ion batteries are currently the most popular on the market, the latest test battery includes a flexible gel polymer electrolyte that allows lithium ions to move between the lithium anode and tellurium cathode. This results in a quasi-solid-state lithium-tellurium battery that has improved performance

✉ Jianzhao Yin
jzyin7@jlu.edu.cn

Yuhong Chao
435975944@qq.com

Haoyu Yin
yinhaoyu11@163.com

Hongyun Shi
hongyunshi@yahoo.com

Shoupu Xiang
shoupx@163.com

¹ Wuhan Institute of Technology, Wuhan 430074, China

² College of Earth Sciences, Jilin University, Changchun 130061, China

³ Ganzhongnan Institute of Geology and Mineral Exploration, Nanchang 330002, China

⁴ Guinea Westfield Mining Company-Sarlu, Jinzhong 031300, China

⁵ Orient Resources Ltd., Richmond, B.C. V7E 1M8, Canada

⁶ Silvercorp Metals Inc., Beijing 100027, China

compared to lithium-sulfur and lithium-selenium batteries (Cheng et al. 2020). The high purity of tellurium along with the metal's overall attributes makes it ideal as a rechargeable battery material.

Even now, the world's leading source of refined tellurium is mainly recovered from Te-bearing minerals including chalcopyrite, etc. As a result, the supply of refined tellurium is very limited (Yin et al. 1995e; Yin 1996a; Yin and Shi 2020a).

So far, the Dashuigou tellurium deposit is the only known independent tellurium deposit in the world. Since its discovery in 1992 (Chen et al. 1993; 1994a, b; Luo and Cao 1994; Luo et al. 1994a, b), its origin has been debated between geologists in China (Cao et al. 1994, 1995; Chen et al. 1994a, b; Chen 1996; Luo et al. 1994a, b, 1996; Wang et al. 1995, 1996, 2000; Yin et al. 1995e; Yin 1996a; Yin and Shi 2020a; Shen et al. 1997; Li et al. 1999, 2000). Chen (1996), Mao et al. (1994, 1995a, b, c) believed that tellurium mineralization is related to the Yanshanian alkaline intrusive rocks, while Luo et al. (1994a, b, 1996) and Liu et al. (1996) believed that the mineralization is related to the Yanshanian granitic magma activity. Yin et al. (1995a, b, 1996a, b) proposed that scattered elements including tellurium and bismuth originated from the mantle's degassing and enriched through nano-effects. Wang et al. (2000) concluded that the deposit was formed on the ancient seafloor by a volcanic eruption in the Late Proterozoic first; the deposit was then strongly superimposed and reconstructed by the Mesozoic multistage regional metamorphic hydrothermal activities.

This article attempts to further explore the origin of the deposit's ore-forming elements through the study of light stable isotopes including carbon, hydrogen, and oxygen, combined with previous research results on the ore-forming source, etc.

2 Regional geology

Nestled in the convergence between the Indian, Eurasian, and Pacific Plates, the Dashuigou tellurium deposit is located in the transitional belt between the Yangtze platform and Songpan-Ganzi folded belt (Xu et al. 1992), as part of the Qinghai-Xizang Plateau (Fig. 1). The crust-mantle structures and properties in the region are the results of cumulative tectogenesis throughout long geological times (Yin 1996a; Yin et al. 2020a, 2022d).

The geophysical data (Luo et al. 1994a, b, 1996; Yin et al. 1994c, 1995d; Yin 1996a, b; Chen 1996; Wang et al. 2000; Yin et al. 2020a, 2022d) indicates that the upper mantle in the region is forming a dome structure.

As a result, the region has the following geophysical properties: high density, high magnetism, high geothermal flow, well-developed earthquakes and mantle's uplift, an

elevated heat flow, a low-velocity and low resistivity zone in the middle crust that is interpreted as a decollement, and an abnormal mantle existing below the crust.

Meanwhile, the region has properties of both geosyncline and platform, as well as special characteristics of its own. It is a geo-tectonically active zone with very complicated structures and igneous rocks.

Overall, this region is geologically very active and a very important south-north trending tectonomagmatic-mineral belt (Luo et al. 1994a, b, 1996; Yin et al. 1994c, 1995d; Yin 1996a, b; Chen 1996; Wang et al. 2000; Yin et al. 2020a, 2022d).

The structures, strata, and igneous rocks in the region trend north-south (Yin et al. 2020a, 2022d).

A large amount of Archaean high-grade metamorphic rocks of the Kangding group emerge to the southeast of the study area. The other strata are low-grade metamorphic rocks of the Silurian, Devonian, and Permian systems, and Middle-Lower Triassic series.

The well-developed igneous rocks in the region are of ultrabasic, basic, neutral, acid, and alkaline types, produced during different geological times.

Various mineral resources including Cu, Pb, Zn, Ti, V, Nb, Ta, Li, REE, rare metals/semi-metals, and coal in the region are very rich; many of which are well known, for instance, the Shimian asbestos and the Panzhihua vanadium titano-magnetite deposit (Luo et al. 1994a, b, 1996; Yin et al. 1994c, 1995d; Yin 1996a, b; Chen 1996; Wang et al. 2000; Yin et al. 2020a, 2022d).

3 Mine geology

The Strata of the mine encompass a set of Lower-Middle Triassic low-grade metamorphic rocks including marble, slate, phyllite, and schist; all of which collectively make up an NNE-trending dome. The tellurium deposit is located at the northeastern end of the Triassic metamorphic dome (Yin et al. 1994c, 1995c).

The ore bodies' main wall and host rocks are schist and phyllite, of which the protolith is poorly differentiated, mantle-derived basalt, which was formed under severe tectonic change with the upper mantle in a non-equilibrium state, based on their geological and geochemical characteristics (Yin et al. 1994a, b, c; 1995d, 1996a, b; Yin 1996a; Yin et al. 2022d) (Fig. 2).

The lithology and lithofacies change significantly and the alteration intensity is different. The alteration within the deposit area is strong and gradually weakens and disappears as it moves away from the deposit. The host rock has undergone multiple tectonic movements, during which faults are developed and various alterations such as dolomitization, tourmalinization, muscovitization,

Fig. 1 Regional geology (after Yin et al. 2022d). 1. The Lower and Middle Triassic metamorphic rocks; 2. The Permian metamorphic rocks; 3. The Devonian metamorphic rocks; 4. Metamorphic rocks of the Siniyan system; 5. The metamorphic base complex of the Archean Kangding group; 6. Plutonic granite of the Indosinian orogeny; 7. Plutonic alkaline syenite of the Indosinian orogeny; 8. Plutonic monzonitic granite of the Indosinian orogeny; 9. Hypabyssal sillite of the Indosinian orogeny; 10. The Late Hercynian basic-ultrabasic rocks; 11. The Late Proterozoic plutonic granite; 12. The Early Proterozoic-Archean plutonic quartz diorite; 13. The deep and large fault; 14. The geological boundary; 15. Village and/or town; 16. The tellurium deposit

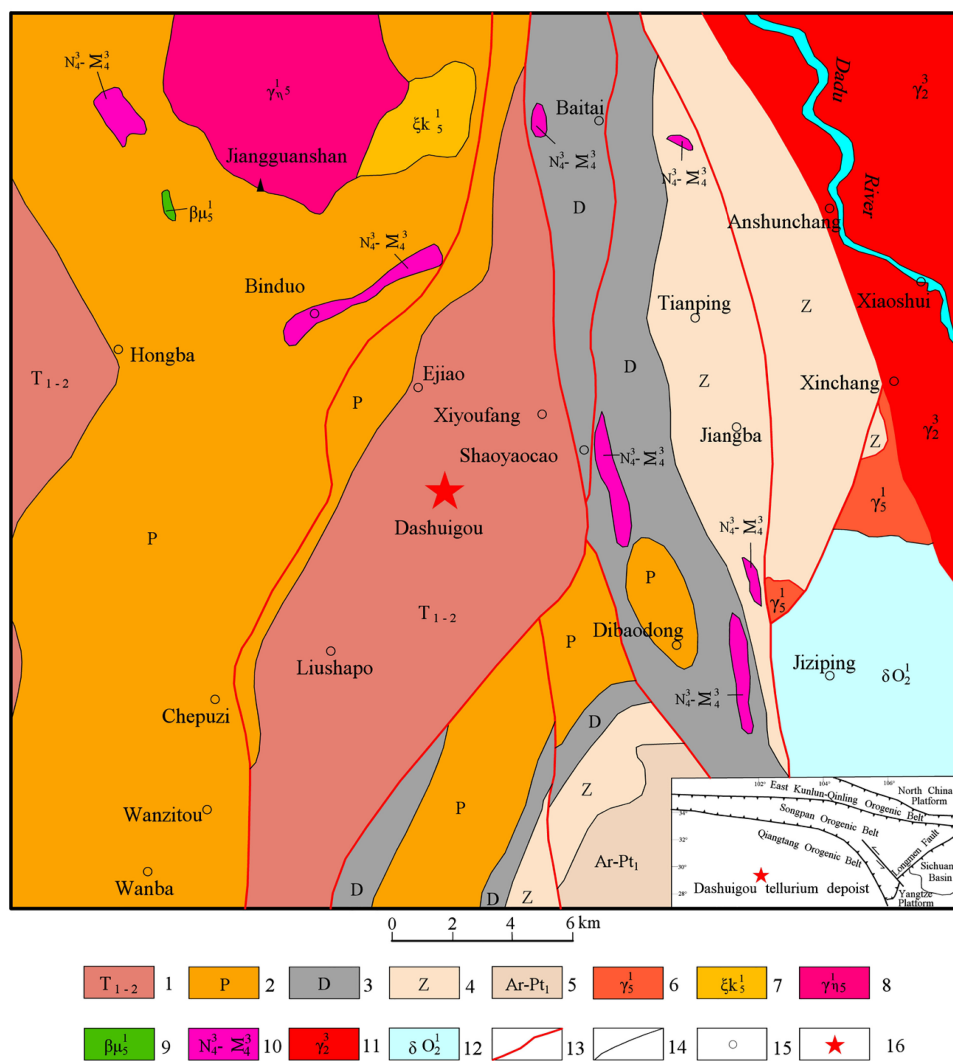
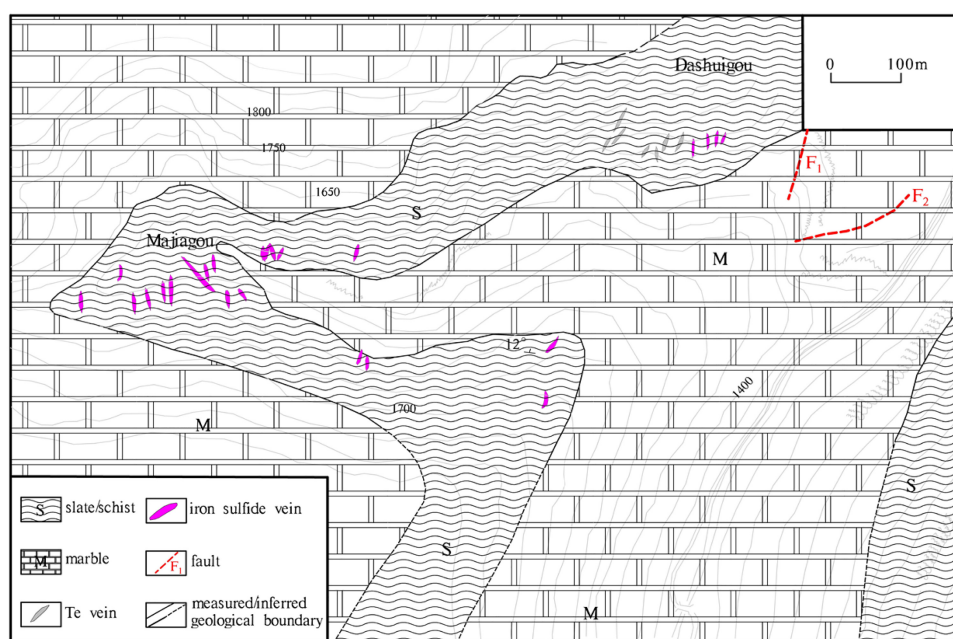


Fig. 2 Mine geology (after Yin et al. 2022d)



silicification, sericitization, and chloritization are commonly seen in the area. More importantly, tellurium, bismuth, gold-silver, lead, copper, pyrite, and pyrrhotite mineralizations are also developed (Yin et al. 2022d).

Both faults and folds are well-developed in the area. Linear faults and circular structures intersected and superimposed with each other to form the special and typical Ø-shaped structures, which control the formation of a variety of mineral deposits, including the Dashuigou tellurium deposit itself, the subject of this article.

No intrusive rocks emerge within 5 km of the deposit. Only two small, Permian ultrabasic-basic rock bodies emerge within a 10 km range of the deposit. The large neutral, acid, and alkaline intrusive bodies exist beyond 10 km of the deposit (Fig. 1).

The ore bodies are controlled by and fill in a group of shear fractures (Figs. 2, 3 and 4). So far, more than nine tellurium ore bodies have been discovered, which strike around 350–10 degrees with a dip of 55–70 degrees towards the west (Figs. 3, 4). The ore bodies' widths vary between 25 and 30 cm. Most of the ore bodies are in the lenticular shape and have sharp contact with their host rocks.

The altered host rocks occur in narrow bands ranging between several centimeters and 1 m in thickness, of which those bands beside the massive ore bodies are narrower and only several centimeters wide.

Among the main alterations mentioned above, dolomitization is the most widely distributed in the area, and the dolomite is symbiotic with sericite and/or muscovite. The early quartz veins developed in dense shear fissures, and

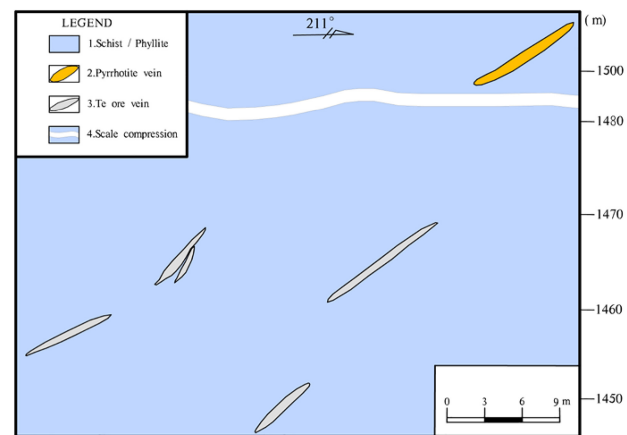


Fig. 4 Longitudinal section of the telluride and pyrrhotite veins of the Dashuigou deposit (modified after Yin 1996a)

the late quartz veins were mostly white with sericite and/or muscovite. Tourmalinization, chloritization, and albitization are closely associated with the early pyrrhotite and pyrite. In general, the wall rock alterations closely related to early pyrrhotite veins include biotitization, dolomitization, silicification, tourmalinization, albitization, chloritization, and pyritization. The typical mineral combination of this early stage is coarse-grained dolomite + coarse-grained pentagonal dodecahedral pyrite + pyrrhotite + biotite + tourmaline + chlorite + quartz. The wall rock alterations closely associated with tellurium veins include muscovitization and/or sericitization, dolomitization, silicification, chalcopyrite, and galena mineralization, etc. The typical mineral combination is tetradyomite + tsumoite + tellurobismuthite + dolomite + quartz + chalcopyrite + native gold + native silver + galena (Figs. 5, 6).

At least 30 minerals including ore minerals such as tetradyomite, tsumoite, tellurobismuthite, gold, silver, and electrum in the ore have been identified. These ore minerals comprise 85% of the deposit's massive and semi-massive ore. Gangue minerals include pyrrhotite, pyrite, dolomite, quartz, chalcopyrite, galena, magnetite, ilmenite, and hematite, with minor calcite, calaverite, siderite, mannesite, rutile, muscovite, biotite, sericite, hornblende, chlorite, plagioclase, K-feldspar, tourmaline, garnet, apatite, and epidote (Yin et al. 1994a, b, c, 1995d, 1996a, b; Chen et al. 1994a, b; Yin 1996a).

The most important ores are massive/semi-massive and the second important ores are disseminated. The tellurium grade in the ores varies between 0.01 and 34.58 wt%.

Replacement, remnant, reaction edge, and granular are the ore's dominant textures; while massive, vein/veinlet, and stockwork vein are the deposit's dominant ore structures. Tetradyomite replaced pyrrhotite and the latter appeared in telluride as a pictographic residue (Fig. 5). Early-formed minerals are often replaced by later-formed minerals and

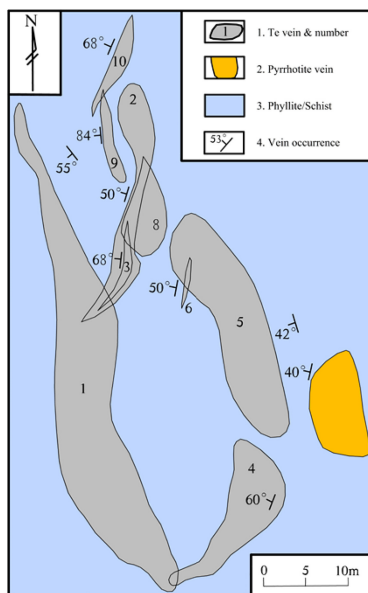


Fig. 3 The horizontal projection of the telluride veins of the Dashuigou deposit (modified after Yin 1996a)

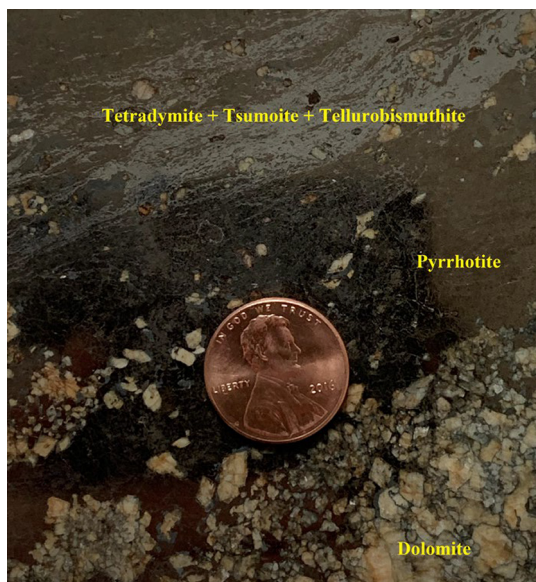


Fig. 5 Light grey-silvery colored tetradymite + tsumoite + tellurobismuthite fine veinlets in massive dark-colored pyrrhotite + dolomite (brownish white) from ore body #I-1 of the deposit

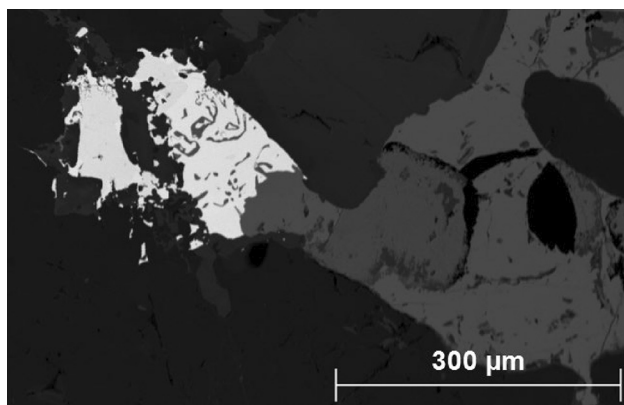


Fig. 6 Solid solution textures between telluride minerals (white) and chalcopyrite (grey)

appear as metasomatic residues. Tetradymite underwent a metasomatic reaction with pyrrhotite to form characteristic reaction edge textures. Solid solution textures between chalcopyrite and tetradymite are common (Fig. 6).

Two paragenetic stages and five sub-stages are recognized in the deposit; namely, the pyrrhotite stage comprising of three sub-stages, dolomite sub-stage → pyrrhotite sub-stage → chalcopyrite sub-stage (from early to late); and the tellurium stage comprising of two sub-stages, tetradymite sub-stage → tsumoite sub-stage (Cao and Luo 1993; Chen et al. 1994a, b; Yin et al. 1995a; Yin 1996a; Mao et al. 1995a, b, c; Xu et al. 1998; Yin and Shi 2020a).

4 Analytical methodology and techniques

Almost all minerals used for isotopic tests in this article were collected and recovered from telluride veins formed during the later tellurium stage, not the earlier pyrrhotite stage, in order to obtain relevant minerals for the tellurium rather than pyrrhotite mineralization stages.

By using an apparatus which was originally used for oxygen isotope analysis through the BrF₅ method, further analyses were conducted, including oxygen isotope analysis of water by means of CO₂-H₂O equilibration, oxygen and carbon isotope analysis of carbonates with H₃PO₄, and deuterium isotope analysis of water using zinc and deuterium-hydrogen composition analysis of water extracted from minerals. The analysis accuracy for the above-mentioned methods was checked against international standards. The analytical results of NBS-18 and NBS-19 are, within the systematical error range, essentially in agreement with the recommended values from various global laboratories. The obtained δD and δ¹⁸O values of NBS-30 agree with those both from I. Fridman and T.B. Coplen (Yichang Institute of Geology and Minerals 1982; Zhang 1989). In addition, the results from the CO₂, water, and oxygen isotope fractionation factor of 1.0417 at 25 °C conform to that from M. Majzoub, and the δ¹⁸O of NBS-28 agrees with that from Y. Matsuhisa (Jin et al. 1985; Jia et al. 2001).

Analysis method of hydrogen and oxygen isotopes in mineral fluid inclusions is summarized as follows:

Weigh 5–15 g sample and wash minerals including quartz and dolomite with concentrated nitric acid to remove other minerals that may be contained. Use deionized water to repeatedly wash to neutral, heat, and dry for standby. Put the samples into a quartz tube, heat it to degas, vacuum it, and place it at a high temperature to burst and collect the fluid. Conduct H and O isotope analysis on the collected fluid. Hydrogen isotopes were determined by the zinc reduction method. Water and zinc exchange under high temperature → hydrogen collection → analysis on a MAT251 mass spectrometry. The determination of oxygen isotopes was by the carbon dioxide-water high-temperature equilibrium method. Oxygen isotope exchange between water and high-purity carbon dioxide at high temperature → collection and exchange of carbon dioxide after equilibrium → MAT 251 mass spectrometry analysis.

The isotope analysis process adopts GBW04402 standard water sample and duplicate sample (30% duplicates of the measured samples). The standard measured value is δD (‰) = −64.8 ± 1.1, δ¹⁸O (‰) = −8.79 ± 0.14, and its certificate value is within the allowable range of measurement error. The test results of duplicate samples are also consistent within the error range, indicating that the test process is reliable and the experimental data obtained are accurate and reliable.

The gases and liquids in the mineral inclusions are released by bursting, crushing, and grinding; and then through separation, purification, and redox reactions to collect testable gases such as hydrogen and carbon dioxide. Finally, a gas isotope ratio mass spectrometer (IRMS) in a dual-injection (duel inlet) mode was used to analyze both carbon and hydrogen isotopes. The analysis error of carbon isotope is generally less than $\pm 1\text{\textperthousand}$.

The laboratories performing isotope testing are listed in the footnotes of Tables 1 and 4.

5 Results

5.1 Carbon and oxygen isotopes

Carbon and oxygen isotope results of dominant carbonate minerals collected from the deposit's various veins and marbles are listed in Table 1 and shown in Fig. 7a, b and c, in which $\delta^{18}\text{O}_{\text{SMOW}}$ is the total oxygen isotope value and is calculated, using the following formula:

$$\delta^{18}\text{O}_{\text{SMOW}} = 1.03086 \times \delta^{18}\text{O}_{\text{PDB}} + 30.86 \quad (\text{Zhang 1984})$$

According to Table 1 and Fig. 7a, b, and c, there exist two different genetic groups of dolomite minerals in the study area:

For dolomite veins outside the deposit, coarse-grained marble and banded marble of the Lower-Middle Triassic strata (series #11 through 13 in Table 1): $\delta^{13}\text{C}$, varies between -0.3 and $-2.1\text{\textperthousand}$ with a range of 2.4 and an average of $1.03\text{\textperthousand}$; $\delta^{18}\text{O}_{\text{PDB}}$ and $\delta^{18}\text{O}_{\text{SMOW}}$ respectively vary between -6.6 and $-3.8\text{\textperthousand}$ and 24.0 – $27.0\text{\textperthousand}$ with respective ranges of $2.8\text{\textperthousand}$ and $3.0\text{\textperthousand}$, and respective averages of $-5.6\text{\textperthousand}$ and $25.1\text{\textperthousand}$. Dolomite veins outside the deposit have very similar carbon and oxygen isotope characteristics to the local marble.

For dolomite veins within the deposit: $\delta^{13}\text{C}$ \textperthousand varies between -7.2 and $-5.2\text{\textperthousand}$ and a 17-sample average of $-5.8\text{\textperthousand}$; and $\delta^{18}\text{O}_{\text{PDB}}$ \textperthousand and $\delta^{18}\text{O}_{\text{SMOW}}$ \textperthousand respectively vary between -20.1 and $-17.3\text{\textperthousand}$ and 10.2 – $13.0\text{\textperthousand}$ with respective averages of $-18.4\text{\textperthousand}$ and $12.90\text{\textperthousand}$.

Both carbon and oxygen isotopes of the two groups of minerals differ greatly, indicating they do not have a genetic relationship with each other; that is, both carbon and oxygen of the deposit's dolomite veins did not derive from the local coarse-grained and banded marbles of the Lower-Middle Triassic strata.

Both carbon and oxygen isotopes of dolomite from the ore veins concentrate in a narrow scope, implying they are from the same source. Figure 8 below demonstrates a similar result of carbon origin as discussed above.

Table 1 Carbon and oxygen isotope results of carbonate minerals from the study area

Series #	Sample ID	Sample name	Location	$\delta^{13}\text{C}_{\text{PDB}}$ (\textperthousand)	$\delta^{18}\text{O}_{\text{PDB}}$ (\textperthousand)	$\delta^{18}\text{O}_{\text{SMOW}}$ (\textperthousand)
1	SD12-1	Dolomite (DV)	Between #II & III Ore Zone	-5.3	-18.7	11.6
2	SD-23	Dolomite (DPyrV)	Next to #I-4 Ore Vein	-5.6	-18.1	12.2
3	SD-29	Dolomite (DPyrV)	Next to #I-5 Ore Vein	-5.5	-18.6	11.7
4	SD-40	Dolomite (DTV)	From #I-1 Ore Vein	-5.6	-18.6	11.7
5	SD-44	Dolomite (DV)	Next to #I-3 Ore Vein	-5.5	-18.0	12.3
6	SD-46	Dolomite (DTV)	From #I-2 Ore Vein	-5.3	-17.4	12.9
7	SD-59	Dolomite (DTV)	From #I-10 Ore Vein	-5.5	-18.0	12.3
8	SD-62	Dolomite (DV)	Next to #I-9 Ore Vein	-5.4	-18.6	11.7
9	SD65-1	Dolomite (DV)	Next to #I-8 Ore Vein	-6.4	-20.1	10.2
10	SD-71	Dolomite (DPyrV)	From #IV Ore Zone	-5.2	-18.4	11.9
11	SL-09	Dolomite (MDV)	At Liushapo next to the mine	2.1	-3.8	27.0
12	SD-49	Calcite from BM	At #4 Portal of the deposit	-0.3	-6.5	24.2
13	SD-69	Calcite from CGM	At bottom of the Dashui Valley	1.3	-6.6	24.0
14	TB-04	Dolomite	Free pickup from the ore stockpile	-7.2	-7.2	12.3
15	TB-05	Dolomite	Free pickup from the ore stockpile	-5.9	-5.9	12.2
16	TB-06	Dolomite	Free pickup from the ore stockpile	-6.2	-6.2	10.9
17	TB-07	Dolomite	Free pickup from the ore stockpile	-5.7	-5.7	11.8
18	TB-08	Dolomite	Free pickup from the ore stockpile	-5.8	-5.8	13.0
19	TB-09	Dolomite	Free pickup from the ore stockpile	-5.7	-5.7	12.4
20	TB-10	Dolomite	Free pickup from the ore stockpile	-6.4	-6.4	12.0

DV Dolomite vein, DPyrV Dolomite–pyrrhotite vein, DTV Dolomite–tetradytmite vein, MDV Muscovite–dolomite

vein, BM Banded marble, CGM Coarse grained marble; uncertainty of these isotope measurements: $\pm 0.1\text{\textperthousand}$;

Lab: Chinese Academy of Geological Sciences

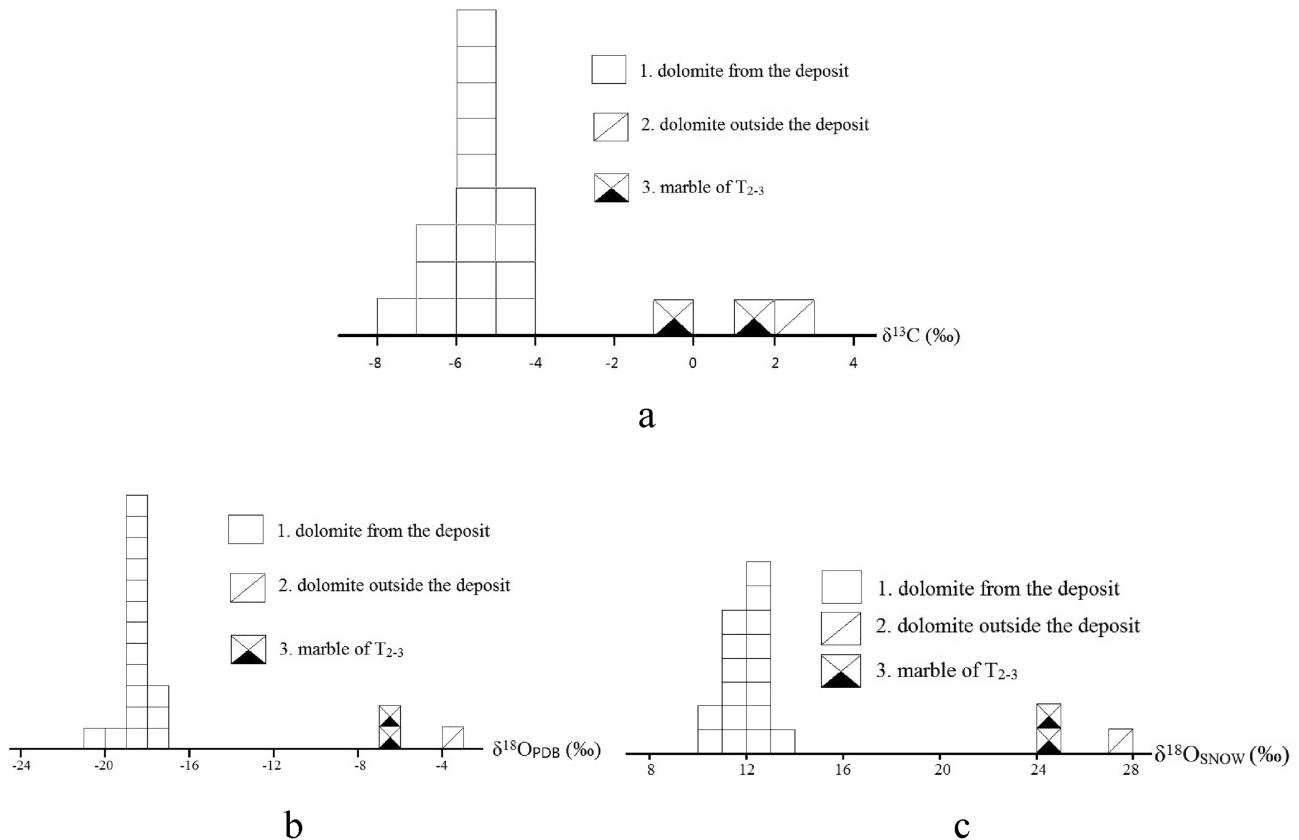
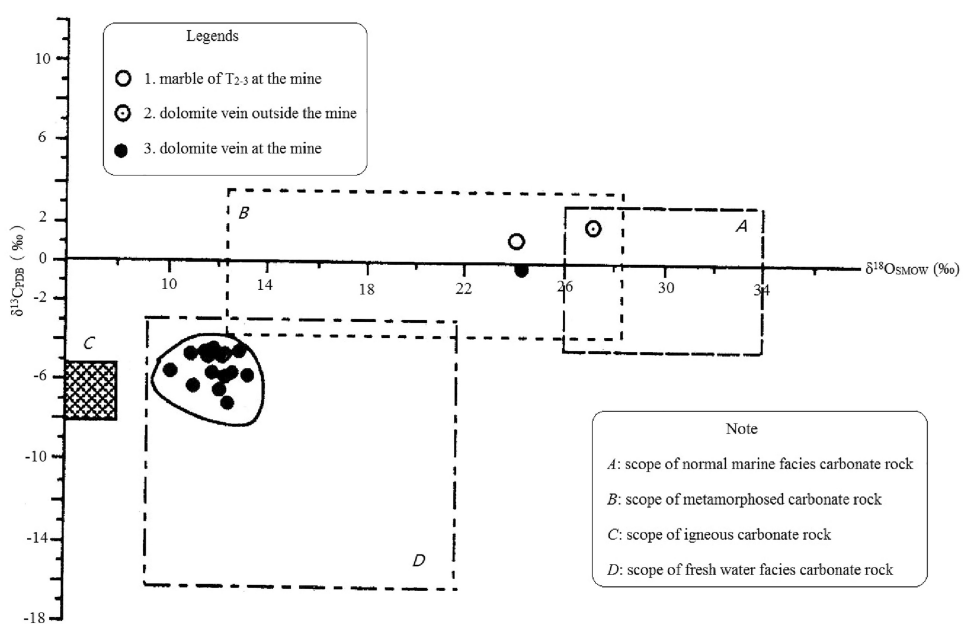


Fig. 7 Histograms of $\delta^{13}\text{C}$ **a**, $\delta^{18}\text{O}_{\text{PDB}}$ **b**, and $\delta^{18}\text{O}_{\text{SMOW}}$ **c** of the main carbonate minerals from the study area

Fig. 8 $\delta^{18}\text{O}_{\text{SMOW}}-\delta^{13}\text{C}_{\text{PDB}}$ diagram indicating carbon and oxygen origins of the carbonate minerals from the study area (the original Fig. was after Zhang 1984)



By comparing the deposit's carbon isotopes with those in Table 2, the authors propose that both the coarse-grained and banded marbles of the Lower-Middle Triassic strata in the

study area represent marine facies, while carbon of dolomite veins outside the deposit are from the marbles. The carbon

Table 2 $\delta^{13}\text{C}$ ‰ characteristics of some typical materials (Yichang 1982)

Organic carbon (‰)	Inorganic carbon (‰)
Aquatic vegetation (−6.0~−19.0)	Diamond (−4.0~−8.0)
General plants (−24.0~34.0)	Graphite −7.5
Algae (−12.0~23.0)	Kimberlite −8.0
Animal (−6.0~−17.0)	Calcite (−4.0~−9.0)
Marine organics −28.0	Volcanic gases (−4.5~−9.0)

Table 3 Z value criteria of carbon origin of the minerals from the study area

Series #	Sample #	Z	Carbon genetic type (source)
1	SD12-1	107.133	Z<120
2	SD-23	106.817	fresh water carbonate
3	SD-29	106.773	
4	SD-40	106.568	
5	SD-44	107.072	
6	SD-46	107.780	
7	SD-59	107.072	
8	SD-62	106.978	
9	SD65-1	104.183	
10	SD-71	107.487	
11	SL-09	129.708	Z>120
12	SD-49	123.449	marine carbonate
13	SD-69	126.676	
14	TB-04	103.590	Z<120
15	TB-05	106.203	fresh water carbonate
16	TB-06	104.941	
17	TB-07	106.413	
18	TB-08	106.806	
19	TB-09	106.712	
20	TB-10	105.079	

of the deposit's dolomite alternations is derived from the mantle.

According to the following equation by Keith et al. via Zhang (1984) and the data from Table 1, Table 3 is produced below:

$$Z = A(\delta^{13}\text{C} \% + 50) + B(\delta^{18}\text{O}_{\text{PDB}} \% + 50).$$

$$A = 2.048, B = 0.498.$$

It is marine facies of carbonate when $Z > 120$, and freshwater facies of carbonate if $Z < 120$.

According to the Z values in Table 3, dolomite carbon in the deposit's ore veins is derived from fresh water, or more precisely, from deep hydrothermal solutions. Those of marbles and dolomite veins outside the deposit are typical marine facies of sedimentary carbonate origin.

The precondition to correctly calculate Z value is that the carbon isotopes did not produce clear fractional

distribution during the geological process (Yichang Institute of Geology and Minerals 1982; Zhang 1984; Sherlock et al. 1995, 1999; Zhang et al. 2013).

5.2 Hydrogen and oxygen isotopes

Hydrogen and oxygen isotope results of quartz, muscovite, biotite, and pyrrhotite in the study area are listed in Table 4. δD of samples SD-20, SD-21, and SD-23 in the table are the result of hydrogen consisting of the minerals, while that of all other samples are the result of H_2O in the corresponding minerals' fluid inclusions.

$\delta^{18}\text{O}$ of different minerals in Table 4 has the following characteristics: $\delta^{18}\text{O}_{\text{quartz}} > \delta^{18}\text{O}_{\text{muscovite}} > \delta^{18}\text{O}_{\text{biotite}}$, which is similar to the $\delta^{18}\text{O}$ of granite minerals after the oxygen isotope exchange is balanced.

δD test of sample #SL-01; namely the sample with the series #1, in Table 4 failed and the sample was destroyed together with its glass tube container. Fortunately, tests of all other quartz samples succeeded, and homogenization temperatures of fluid inclusions in those samples were obtained. By using the following equation by Clayton and O'Neil (1972), as well as both homogenization temperatures of fluid inclusions and $\delta^{18}\text{O}_{\text{SMOW}}$ of the corresponding minerals, $\delta^{18}\text{O}_{\text{H}_2\text{O}}$ of the hydrothermal solutions that have reached oxygen exchange balance with the corresponding minerals are calculated and displayed in Table 4.

$$1000\ln a = 3.38 \times 10^6 T^{-2} - 3.40.$$

$$1000\ln a \approx \delta^{18}\text{O}_{\text{quartz}} - \delta^{18}\text{O}_{\text{H}_2\text{O}}.$$

$$\text{Namely, } \delta^{18}\text{O}_{\text{quartz}} - \delta^{18}\text{O}_{\text{H}_2\text{O}} = 3.38 \times 10^6 T^{-2} - 3.40.$$

$\delta\text{D}\%$ of all samples in Table 4 varies between −134 and −59 ‰ with a 10-sample average of −72.4 ‰. According to the traditional hydrogen isotope theory, δD of the study area's quartz and biotite fall into Taylor's (1968) magmatic water area ($\delta\text{D} = -50$ and -85 ‰), while that of pyrrhotite belongs to Taylor's meteoric water range. Additionally, δD of the samples overlaps with that of metamorphic water (−20 and -90 ‰) (Taylor 1968; Yichang Institute of Geology and Minerals 1982; Zhang 1984). Figure 9 below also shows the origins of the metallogenetic fluids.

Oxygen isotope results of dolomite and calcite are respectively listed in Tables 1 and 4, as discussed earlier in this paper, and further summarized in Table 5.

From Table 5, it can be seen that:

$$\delta^{18}\text{O}_{\text{dolomite (outside the mine)}} > \delta^{18}\text{O}_{\text{calcite (of the mine)}} > \delta^{18}\text{O}_{\text{quartz (vein)}} \geq \delta^{18}\text{O}_{\text{dolomite (of the mine)}} > \delta^{18}\text{O}_{\text{muscovite (of the mine)}} > \delta^{18}\text{O}_{\text{biotite}} > \delta^{18}\text{O}_{\text{quartz (granite)}}.$$

By use of the following equations, $\delta^{18}\text{O}_{\text{H}_2\text{O}}$ of dolomite and calcite can be obtained and are listed in Table 6 and shown in Fig. 10 below:

Table 4 δD and $\delta^{18}\text{O}$ results of minerals from the study area

Series #	Sample id	Sample name	Location	H.T °C	δD_{SMOW} ‰	$\delta^{18}\text{O}_{\text{SMOW}}$ ‰	$\delta^{18}\text{O}_{\text{H}_2\text{O}}$ ‰
1	SL-01	Quartz from granite	At Niubeishan, Xinchang outside the deposit	n/a	n/a	8.5	n/a
2	SL-06	Quartz from a QV	At Liushapo outside the deposit	291.3	-72.0	17.8	10.59
3	SL-11	Quartz from a TQV	At Liushapo outside the deposit	339.0	-61.0	13.8	8.18
4	SD-09	Quartz from a QV	From #II-1 Ore Zone	180.0	-82.0	13.4	0.33
5	SD12-1	Quartz from a QV	Between #II & III Ore Zones	415.3	-62.0	12.9	9.17
6	SD-25	Quartz from ore	From #I-4 Ore Vein	225.0	-64.0	13.4	3.17
7	SD-67	Quartz from ore	From #I-7 Ore Vein	337.7	-59.0	12.3	6.64
8	SD-20	Biotite from A.R	at the footwall of #III-3 Pyrrhotite Vein	n/a	-67.0	8.6	n/a
9	SD-21	muscovite From A.R	at the footwall of #III-3 Pyrrhotite Vein	n/a	-64.0	11.4	n/a
10	SD-23	muscovite From A.R	Next to #I-4 Ore Vein	n/a	-59.0	10.2	n/a
11	SD-34	Pyrrhotite	Next to #I-4 Ore Vein	n/a	-134.0	n/a	n/a

H.T. Homogenization temperature, QV Quartz vein, A.R. Altered wall-rock, TQV Tourmaline-quartz vein

Lab: Analysis by Chinese Academy of Geological Sciences

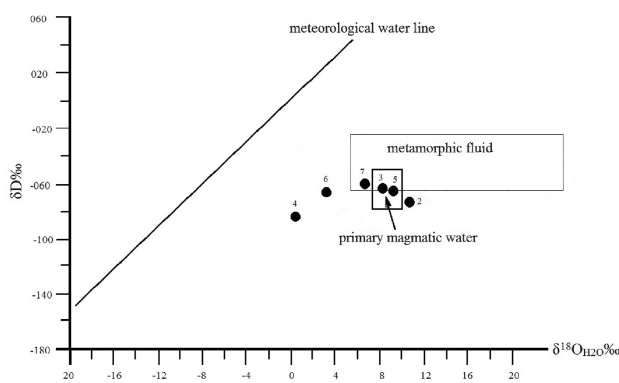


Fig. 9 δD - $\delta^{18}\text{O}_{\text{H}_2\text{O}}$ diagram of quartz demonstrating fluid origins of the study area (Spot numbers on the diagram corresponding to the sample series numbers in Table 4). 2: SL-06, 3: SL-11, 4: SD-09, 5: SD-12-1, 6: SD-25, 7: SD-67

$$1000\ln a = 3.08 \times 10^6 T^{-2} - 3.24 \text{ (for dolomite)} \text{ (Zhang 1984).}$$

$$1000\ln a \approx \delta^{18}\text{O}_{\text{dolomite}} - \delta^{18}\text{O}_{\text{H}_2\text{O}}.$$

And,

$$1000\ln a = 2.78 \times 10^6 T^{-2} - 3.39 \text{ (for calcite)} \text{ (Zhang 1984).}$$

$$1000\ln a \approx \delta^{18}\text{O}_{\text{calcite}} - \delta^{18}\text{O}_{\text{H}_2\text{O}}.$$

$\delta^{18}\text{O}_{\text{H}_2\text{O}}\text{‰}$ of the deposit is similar to both that of the Providencia Pb-Zn deposit in Mexico (0.2–7.0‰) and that of the Casapalace Ag-Pb-Zn mine in Peru (4.0 – 10.0 ‰), both of which are believed to be of typical magmatic water origin (Yichang Institute of Geology and Minerals 1982; Ding et al. 2013; Gammons et al. 2020; Quesnel et al. 2023 and Cherai et al. 2023).

Based on the data above, the authors preliminarily conclude that $\delta D\text{‰}$, $\delta^{18}\text{O}$, and $\delta^{18}\text{O}_{\text{H}_2\text{O}}$ of dolomite, quartz, pyrrhotite, muscovite, and biotite indicate that the deposit's metallogenetic hydrothermal solutions are primarily mantle-derived.

Table 5 Summarized characteristics of $\delta^{18}\text{O}$ of minerals from the study area

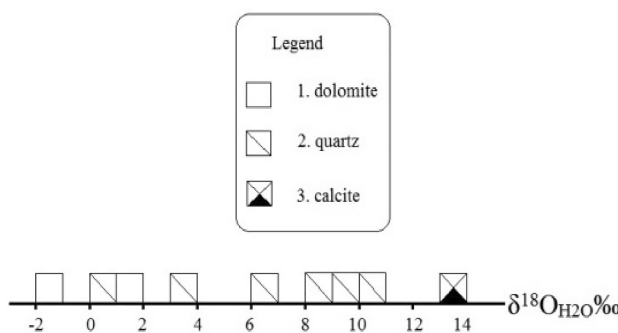
Mineral	# of sample	$\delta^{18}\text{O}_{\text{SMOW}}$ (‰)			
		Scope	Range	Concentrated modal value	Average
Calcite	2	24.0 ~ 24.2	0.2	n/a	24.1
Dolomite from the deposit	17	10.2 ~ 13.0	2.8	11.6 ~ 12.4	12.0
Quartz from a quartz vein	6	12.3 ~ 17.8	5.5	12.3 ~ 13.8	13.9
Muscovite	2	10.2 ~ 11.4	1.2	n/a	10.8
Biotite	1	8.6	n/a	8.6	8.6
Quartz from granite	1	8.5	n/a	8.5	8.5
Dolomite from outside the deposit	1	27.0	n/a	n/a	27.0

Table 6 Calculated $\delta^{18}\text{O}_{\text{H}_2\text{O}}$ of dolomite and calcite from the study area

series #	sample id	H.T. (°C)	$\delta^{18}\text{O}_{\text{SMOW}}\text{‰}$	$\delta^{18}\text{O}_{\text{H}_2\text{O}}$
8	SD-62	165.0	11.7	-1.11
9	SD65-1	238.0	10.2	1.64
13	SD69	180.7	24.0	13.88

H.T. Homogenization temperature of fluid inclusions

Sample series # in the table is same as those in Table 1

**Fig. 10** Histogram of $\delta^{18}\text{O}_{\text{H}_2\text{O}}$ of the main minerals from the study area

6 Discussion

The carbon and oxygen isotope research results of this article confirm that there are two groups of carbonate minerals in the study area that are not genetically related. By comparing the deposit's carbon isotopes with those in Table 2, we propose that both the coarse-grained and banded marbles of the Lower-Middle Triassic strata in the study area are marine facies, while carbon of dolomite veins outside the deposit is from these marbles. Both carbon and oxygen isotopes of dolomite from the ore veins concentrate in a narrow scope, implying they are from the same source. Figure 8 above demonstrates a similar if not the same result of carbon origin.

On the basis of the very brief discussion above, our preliminary conclusion is that the T_{1-2} marbles in the study area are metamorphosed marine facies of carbonate rocks. The dolomite veins, which are one of the major Te-carriers, show highly uniform isotopic signatures and their average $\delta^{13}\text{C}_{\Sigma\text{C}}\text{‰}$ and $\delta^{18}\text{O}_{\Sigma\text{O}}\text{‰}$ values are similar to the general total carbon $\delta^{13}\text{C}_{\Sigma\text{C}}\text{‰}$ and total oxygen $\delta^{18}\text{O}_{\Sigma\text{O}}\text{‰}$ of the deposit's metallogenetic solutions, meaning these Te-carrying dolomite veins have nothing to do with the T_{1-2} marbles. Moreover, they imply that they are mantle-derived and were produced by the abnormal mantle zone as CO_2 degassed from the deep Earth, and have no relation to the wall rocks in

the area (Yin and Shi 2020a; Yin et al. 2022d). Meanwhile, both carbon and oxygen of those dolomite veins outside the deposit mainly derive from the marbles of the country rocks.

$\delta\text{D}\text{‰}$, $\delta^{18}\text{O}$, and $\delta^{18}\text{O}_{\text{H}_2\text{O}}$ of dolomite, quartz, pyrrhotite, muscovite, and biotite from the mine show that the deposit's metallogenetic hydrothermal solutions are mainly mantle-derived. Dolomite veins outside the deposit have very similar carbon and oxygen isotope characteristics to the marbles, meaning both carbon and oxygen of the dolomite veins outside the deposit resulted from the local marbles in the area.

According to Yin and Shi (2020a), $\delta^{34}\text{S}\text{‰}$ of tetradytmite from the deposit is similar to that of meteorites and rocks from the mantle, indicating that the sulfur originates from the mantle. In addition, lead isotopes of the telluride minerals indicate that the deposit's lead is primarily from the mantle with some captured from the Earth's crust.

It is worth discussing the true meaning of sample SD-34's δD value: -134.0‰ of pyrrhotite in Table 4, as this kind of value was traditionally considered to be of meteoric origin. In the 1980s-1990s, many geologists already observed δD of mantle-derived solutions as low as below -250.0 (Nabelek et al. 1983; Taylor 1983; Taylor et al. 1984; Brigham and O'Neil 1985; Sheppard and Harris 1985; Qin et al. 1987; Yu et al. 1989; Gui et al., 1989; Li & Yu 1989; Li & Shen 1990; Li et al. 1992; Chen 1993, 1996). They believed that magmatic degassification or dewatering could result in such low δD values. Chen (1993, 1996) stated that negative δD values indicate a close relationship with the Earth's evolution, during which hydrogen isotopes respectively experienced open, semi-open, and closed system fractionations, and resulted in isotope differentiation between the hydrosphere, lithosphere, and mantle. Additionally, the fractionation degree of hydrogen isotopes increases as the depth to the Earth's core increases. The higher the fractionation degree of hydrogen isotopes, the lower the δD values; that is, a mantle-derived solution could have extremely low δD values. Research on hydrogen isotopes of both fluid inclusions of meteorite and of the solar system already proves this (Robert et al. 1979, 1981, 1983; Yang et al. 1982a, b, 1983; and Pillinger 1984). Examples of this include: δD , $\delta^{18}\text{O}$, and $\delta^{18}\text{O}_{\text{H}_2\text{O}}$ of 4 alkaline riebeckite samples of the Bayan Obo Giant REE mine in China, which were believed to be mantle-derived, are respectively -227.4, 6.9, and 0.9; -230.3, 6.8, and 1.3; -243.1, 8.51, 1.2; and -253.9, 8.6, and 0.7. δD and $\delta^{18}\text{O}$ of the brucite sample collected from the mantle-derived ultrabasic intrusive of the well-known asbestos mine close to the Dashuigou tellurium deposit are respectively -128.3 and -9.4 ‰ (Xu and Li 1987).

As a result, the $\delta\text{D}\text{‰}$ value -134 of the pyrrhotite sample numbered SD-34 in Table 4 may indicate mantle-derived water, but not meteoric water.

Cao et al. (1994, 1995) published oxygen isotope results for the same deposit of 6.1–7.91‰, though neither the kinds

of minerals contained within these samples nor whether the oxygen isotope was $\delta^{18}\text{O}_{\text{mineral}}$ or $\delta^{18}\text{O}_{\text{H}_2\text{O}}$ were discussed. Cao et al. concluded that the isotope results showed magmatic water characteristics, and also published $\delta^{18}\text{O}_{\text{H}_2\text{O}} \text{‰}$ and $\delta\text{D} \text{‰}$ of quartz samples from the late quartz veins, which were respectively 1.28–8.70 and –56.40––146.45, and concluded that meteoric water got involved in the later mineralization epoch.

Our study shows that $\delta^{18}\text{O}_{\text{quartz (vein)}} \text{‰}$ concentrates between 11.6 and 12.4, very close to that of $\delta^{18}\text{O}_{\text{muscovite}}$ of the mine, implying they were from the same source.

According to Chen (1993, 1996), similar to hydrogen and other stable isotopes mentioned above, stable isotope values decrease with closer proximity to the Earth's core; for instance, $\delta^{18}\text{O}$ of sedimentary rocks is higher than that of igneous rocks. Meanwhile, heavy stable isotopes tend to enrich at the Earth's surface while light ones enrich at the Earth's core, and in the same hydrothermal solution system, $\delta^{18}\text{O}$ of early-formed minerals is lower than that of late-formed ones due to further fractionation of the stable isotopes. This explains why $\delta^{18}\text{O}_{\text{dolomite}}$ outside the mine is higher than that of other minerals in the region because it results from the marble of the country rocks.

According to previous researchers, the deposit's ore-forming fluid can be divided into the magma hydrothermal origin (Cao et al. 1994, 1995; Luo et al. 1994a, b, 1996; Chen 1996; Chen et al. 1998; Li et al. 1999; Li and Liu 2000), the metamorphic hydrothermal origin (Wang et al. 1995; Shen et al. 1997), and the mixed hydrothermal origin (Wang et al. 2000).

By studying the gas–liquid inclusions in minerals from the deposit, Luo et al. (1994a, b) and Wang et al. (1995) derived the following physical and chemical conditions for the deposit's mineralization: the ore-forming temperature 120–350 °C, the salinity 7.2–35.0 wt% NaCl, the oxygen fugacity $f_{\text{O}_2} = -42.3$ to -45.5 , and the pH of ore-forming hydrothermal fluid 6.3. Unfortunately, their study did not specify which mineralization stage the minerals were taken from. Therefore, these data are only for reference.

Similarly, Cao et al. (1994, 1995) and Li et al. (1999) obtained the following physical and chemical conditions for the mineralization: the corrected paragenetic temperatures of stages I, II, and III were 319, 315, and 304 °C, respectively; an average paragenetic pressure of $884 \times 10^5 \text{ Pa}$ and the corresponding paragenetic depth estimated by the static rock pressure model 3339 m. Since the inclusion types in each mineralization stage are pretty similar, they are considered to have similar paragenetic depths. It should still be noted that such numbers are not accurate (Pei et al. 2016; Xu et al. 2016). The salinity of fluids from each mineralization stage is roughly similar, with an average of 21% in stage I, 26% in stage II, and 18% in stage III, respectively. The pressures of the mineralization fluids respectively are stage

I 10.0×10^5 –34.0 $\times 10^5 \text{ Pa}$, stage II 10.0×10^5 –34.8 $\times 10^5 \text{ Pa}$, and stage III 10.0×10^5 –35.6 $\times 10^5 \text{ Pa}$. The pH value of the hydrothermal solution during the tellurium mineralization stage is 5.9, which is estimated by using alkali metal ions and halogen element ions (Pei et al. 2016; Xu et al. 2016).

Also by their study of gas–liquid inclusions from the same deposit, Chen et al. (1998) concluded that three systems of fluid inclusions exist in the deposit, of which tellurium mineralization is related to the first two systems. The paragenetic temperature of the tellurium stage is 400 °C, the fluid density varies between 1.0 and 0.76 g/cm³, and the paragenetic pressure is 240–300 MPa.

According to Yin and Shi (2021b), fluid inclusions are different in different host minerals from the deposit. Fluid inclusion homogenization temperatures of those quartz samples formed during the tellurium stage vary between 180 and 250 °C. The salinity of fluid inclusions in minerals formed during the tellurium stage is between 15 and 19 wt% NaCl eq. within the medium salinity range, while formation pressures of the samples from minerals formed during the tellurium stage vary between 0.65 and 1.02 Kbar. The saturation pressure of the gas phase when the liquid-rich inclusions are homogeneous is obtained by projection on the T-w-ρ phase diagram of Bischoff & Metzler (1991), and the pressure range is determined by the intersection of the homogenization temperature and salinity curves. The uniform pressure of CO₂-rich inclusions is obtained by looking up the related table. The corresponding mineralization depth is 4.1–2.2 km, while mineralization temperatures of the deposit's tellurium stage are 216.9–229.0 °C. The fluid inclusions are richest in SO₄²⁻, richer in H₂O than in CO₂, rich in Ca²⁺, CO₂, H₂, and CH₄, and moderate in Cl⁻.

After Wei and Mao (1998) and Chen et al. (1998) conducted similar studies on relevant fluid inclusions of the deposit, they concluded that the ore-forming fluids and elements are mantle-derived.

The results of quantitative chemical analysis of the abundance of mineralizing elements in the surrounding rocks in the study area indicate that these surrounding rocks are not ore-forming sources. In other words, the ore-forming elements are not derived from relevant strata and igneous rocks in the study area (Yin et al. 1994a, b, c; 1995d, 1996a, b; Yin 1996a). Earlier studies have shown that ore-forming elements come from the mantle (Yin and Shi 2020a; Yin et al. 2022d).

Considering both the geology and geochemistry of the ore bodies, the deposit's ore veins cut across metamorphic wall-rocks but do not emplace along the beddings, meaning that the metallogeny has nothing to do with metamorphic fluid, but instead has a close relationship with the fluids degassed from the mantle which mixed with some meteoric water (Yin and Shi 2019a, 2020a, Yin et al. 2022d). The deposit

is formed by fluids rich in nano-scale substances including Fe, Te, S, As, Bi, Au, Se, H₂, CO₂, N₂, H₂O, and CH₄, which are degassed from the mantle during the Himalaya orogeny and enriched by nano-effect, and finally rise to a certain part of the crust along the lithospheric fault to form the deposit (Yin and Shi 2019a; Yin et al. 2022d).

7 Conclusions

The carbon, hydrogen, and oxygen related to the Dashuigou tellurium deposit derive from the upper mantle.

The deposit's formation results from the Himalayan orogeny. During the late Mesozoic and Cenozoic periods, the Tethyan region including Qinghai-Xizang between Gondwanaland and Eurasia underwent closure and deformation, culminating with the upheaval of the Himalayas, Alps, and other mountain ranges in Asia Minor. During this series of main tectonic–magmatic events, tellurium, bismuth, sulfur, and hydrothermal solutions from the upper mantle gathered together and enriched gradually. Meanwhile, these materials moved upward and finally formed the tellurium deposit unique in the world.

As a noteworthy new perspective based on numerous earlier studies, it has to be noted the mantle-derived ore-forming solutions could have extremely low δD values, due to the fractionation of hydrogen isotope.

8 Additional information

Correspondence and requests for materials should be addressed to Prof. Dr. J. Yin (jimyin7@yahoo.ca), please.

Acknowledgements Support for this study was received from Orient Resources Ltd. in Canada, Wuhan Institute of Technology, China, and College of Earth Sciences, Jilin University, China. Additional support was provided respectively by Prof. R.F. Pei of the Chinese Academy of Geological Sciences, also an Academician of the Chinese Academy of Engineering, and Prof. J.X. Zhou of the Chinese Academy of Geological Sciences of China, both of whom provided insightful discussions of this manuscript. The measurements and chemical analyses included in this article were carried out in the labs of the Chinese Academy of Geological Sciences in Beijing. The authors very much appreciate the time invested respectively by Mr. D.S. Yin and Mr. M. Storey, M. Eng. and P. Eng. with APEGBC of Canada, for their review and editorial work on this contribution.

Author contributions The entire study included in the paper was proposed and organized by JY and YC, who should be regarded as co-first authors. Most of the figures and tables were prepared by HY and HS, who also helped the two co-first authors with the whole research. HS and SX helped complete part of the chemical analyses. All authors prepared and reviewed the manuscript and approved the final version.

Data availability The data that support the findings of this study is available from the authors upon reasonable request.

Declarations

Conflict of interest The authors declare no competing interests.

References

- Bischoff A, Metzler K (1991) Mineralogy and petrography of the anomalous carbonaceous chondrites Yamato-86720, Yamato-82162, and Belgica-7904. In: Fifteenth Symposium on Antarctic Meteorites. Proceedings of the NIPR Symposium, No. 4: 226–246.
- Brigham RH, O'Neil JR (1985) Genesis and evolution of water in a two-mica pluton: a hydrogen isotope study. *Chem Geol* 49(1–3): 159–177.
- Cao ZM, Wen CQ, Li BH (1995) Genesis of the Dashuigou tellurium deposit in Sichuan Province of China. *Sci China (B)* 25(6):647–654 (**in Chinese with English abstract**).
- Cao ZM and Luo YN (1993) Geological characteristics and material composition of the Shimian Te(Se) deposit in Sichuan province. In: Proceedings of the Fifth National Conference on Mineral Deposits. Beijing: Geological Publishing House, 476 (**in Chinese**).
- Cao ZM and Luo YN (1994) Mineral sequence and ore genesis of the Sichuan telluride lode deposit in China. In: New research progresses of the mineralogy, petrology and geochemistry in China. Lanzhou: Lanzhou University Publishing House, 476–478 (**in Chinese**).
- Chen YC, Yin JZ, Zhou JX (1994a) The first and only independent tellurium ore deposit in Dashuigou, Shimian county, Sichuan province. *China Sci Geol Sinica* 3(1):109–113 (**in Chinese with English abstract**).
- Chen YC, Yin JZ, Zhou JX (1994b) Geology of the Dashuigou independent tellurium deposit of Sichuan Province. *Acta Geosci Sin* 29(2):165–167 (**in Chinese with English abstract**).
- Chen PR, Lu JJ, Wang RC, Xu SJ, Chen XM (1998) Study on the fluid inclusions of the Dashuigou independent tellurium deposit in Shimian county, Sichuan province, China. *Mineral Deposit* 17:1011–1014 (**in Chinese with English abstract**).
- Chen YC, Mao JW, Zhou JX, Yin JZ (1993) Dashuigou tellurium gold deposit in Shimian county, Sichuan province—the world's first independent tellurium deposit mainly composed of tellurium. In: Proceedings of the fifth national conference on mineral deposits. Beijing: Geological Publishing House, 437–439 (**in Chinese**).
- Chen YC, Mao JW, Luo YN, Wei JX, Cao ZM (1996) Geology and geochemistry of the Dashuigou tellurium (gold) deposit in western Sichuan, China. Beijing: Atomic Energy Press, 146 (**in Chinese with English abstract**).
- Chen H (1993) Fractionation of stable isotopes during the Earth's forming and evolution. In: Isotope geochemistry of the crust–mantle evolution, diagenesis, and mineralization. Beijing: Seismic Publishing House (**in Chinese**).
- Chen H (1996) Isotope fractionation of hydrogen during Earth's evolution. *Scientia Geologica Sinica* 31(3):238–248 (**in Chinese with English abstract**).
- Cheng ZY, Zhu XM, Zeng Y (2020) Current status of tellurium extraction and utilization. *Mineral Protect Utilizat* 40(5):76–89 (**in Chinese**).

- Cherai M, Rddad L, Talbi F, Walter BF (2023) Trace-element geochemistry and S–O isotopes in the fluorite barite mineralization of Merguechoum, Moroccan eastern Meseta: insights into ore genesis to the Pangea rifting. *Acta Geochimica* 42:435–452. <https://doi.org/10.1007/s11631-022-00592-5>
- Clayton RN, O’Neil JR, Mayeda TK (1972) Oxygen isotope exchange between quartz and water. *J Geophys Res* 77:3057–3067. <https://doi.org/10.1029/jb077i017p03057>
- Ding QF, Jiang SY, Sun FY, Qian Y, Wang G (2013) Origin of the Dachang gold deposit, NW China: constraints from H, O, S, and Pb isotope data. *Int Geol Rev* 55(15):1885–1901. <https://doi.org/10.1080/00206814.2013.804687>
- Gammoms CH, Korzeb SL, Hargrave PA (2020) Metallic ore deposits of Montana. MBMG special publication 122: Geology of Montana 2: Special Topics.
- Gui X, Cheng Z, Yu F, Yu J (1989) Study on isotope geochemistry of the Laoshan geode alkaline granite in Qingdao, China. *Acta Petrologica Sinica* 4:37–44 (in Chinese with English abstract).
- Jia YF, Li X, Kerrich R (2001) Stable isotope (O, H, S, C, and N) systematics of quartz vein systems in the turbidite-hosted central and north Deborah gold deposits of the Bendigo goldfield, central Victoria, Australia: Constraints on the origin of ore-forming fluids. *Econ Geol* 96(4):705–721. <https://doi.org/10.2113/gseco96.4.705>
- Jin SJ, Li JC, Wang CY, Wan DF, Wang MY (1985) Comprehensive test for stable isotope of oxygen, hydrogen and carbon and determination of reference samples. *Bull Chin Acad Geol Sci.* 11:89–102 (in Chinese with English abstract).
- Li T (1976) Abundance of chemical elements in the Earth. *Geochemistry*. 3:167–174 (in Chinese).
- Li BH, Cao ZM, Jin JF, Wen CQ (1999) Physicochemical conditions of the tellurium deposit in Dashuigou. *China Scientia Geologica Sinica*. 34(4):463–472 (in Chinese with English abstract).
- Li BH, Cao ZM, Wen CQ (2000) Fluid inclusion type and geological characteristics of the Dashuigou tellurium deposit in Sichuan Province, China. *Bull Mineral Petrol Geochem.* 4:346–347 (in Chinese with English abstract).
- Li P, Yu J (1989) Hydrogen and oxygen isotope composition of the Shanaiguan geode alkaline granite. *Sci Bulletin* 34(1):51–52 (in Chinese with English abstract).
- Li P, Shen Y (1990) ^{18}O contours of the Nianzishan geode alkaline granite in Heilongjiang Province of China and ancient fossils. *Chinese Sci (8)*:862–869 (in Chinese with English abstract).
- Li P, Yu F, Liu D, Yu J (1992) Hydrogen isotope composition and magma degassing of the Nianzishan geode alkaline granite in Heilongjiang Province of China. *Geochemistry* 1:70–76 (in Chinese with English abstract).
- Liu AP, Zhong ZC, Tang JW (1996) Geochemical characteristics of the Dashuigou tellurium deposit in Sichuan province of China. *Geochemistry*. 25(4):365–371 (in Chinese with English abstract).
- Luo YN, Cao ZM (1994) The world’s first independent tellurium deposit was discovered in Sichuan Province. *China Geol.* 2:27–28 (in Chinese with English abstract).
- Luo YN, Fu DM, Zhou SD (1994a) Genesis of the Dashuigou tellurium deposit in Sichuan Province of China. *Bull Sichuan Geol.* 14(2):101–110 (in Chinese with English abstract).
- Luo YN, Fu DM, Zhou SD, Cao ZM, Li DH (1994b) Geology and genesis of the Dashuigou tellurium deposit in Shimian county, Sichuan province. *Sichuan Geol J.* 14(2):1–10 (in Chinese with English abstract).
- Luo YN, Cao ZM, Wen CQ (1996) Geology of the Dashuigou independent tellurium deposit, Chengdu. Southwest Communication University Publishing House, 30–45 (in Chinese with English abstract).
- Mao JW, Chen YC, Yang BC, Lei YF, Zhou JX (1995a) Study on tetracydymite in Dashuigou tellurium polymetallic deposit, Shimian county, Sichuan province. *China Geol Sci* 30(1):47–52 (in Chinese with English abstract).
- Mao JW, Chen YC, Zhou JX (1995b) Geology, mineralogy, petrology, and geochemistry of the Dashuigou tellurium deposit in Shimian county, Sichuan province, China. *Acta Geosci* 2(3):276–290 (in Chinese with English abstract).
- Mao JW, Wei JX, Yang BC (1995c) A preliminary study on the genesis of the Dashuigou tellurium deposit in Shimian county, Sichuan province, China. *Bull Mineral Petrol Geochem* 1:23–24 (in Chinese with English abstract).
- Mao JW, Chen YC, Yang BC, Zhou JX, Yin JZ (1994) Important progress has been made in the study of Dashuigou tellurium polymetallic deposit in Shimian county, Sichuan province. *Mineral Deposit*. 13(1): back cover.
- Nabelek PI, O’Neil JR, Papike JJ (1983) Vapor phase exsolution as a controlling factor in hydrogen isotope variation in granitic rocks: the Notch Peak granitic stock, Utah. *Earth Planet Sci Lett* 66:137–150. [https://doi.org/10.1016/0012-821X\(83\)90132-2](https://doi.org/10.1016/0012-821X(83)90132-2)
- Pei YR, Sun QZ, Zheng YC, Yang ZS, Li W, Huang KX (2016) Genesis of the Bangbu orogenic gold deposit, Tibet: Evidence from fluid inclusion, stable isotopes, and Ar-Ar geochronology. *Acta Geol Sin* 90(2):722–737. <https://doi.org/10.1111/1755-6724.12700>
- Qin ZW, Yu F, Yu JS (1987) D/H evidence for magmatic degassing of miarolitic alkaline granites in Kuiqi and Qingdao. *China Geochem J* 21(4):149–157. <https://doi.org/10.2343/geochemj.21.149>
- Quesnel Q, Scheffer C, Beaudoin G (2023) The light stable isotope (hydrogen, boron, carbon, nitrogen, oxygen, silicon, sulfur) composition of orogenic gold deposits. In: Isotopes in economic geology, metallogenesis and exploration. 283–328.
- Shen WZ, Xu XJ, Wang RC (1997) Origin of the fluid inclusions of the Dashuigou tellurium deposit in Sichuan Province, China – hydrogen and oxygen isotope evidence. *J Nanjing University (Natural Sciences)* 33 (special issue), 77–83 (in Chinese with English abstract).
- Sheppard SMF, Harris C (1985) Hydrogen and oxygen isotope geochemistry of Ascension Island lavas and granites: variation with crystal fractionation and interaction with sea water. *Contrib Miner Petrol* 91:74–81
- Sherlock RS, Tosdal RM, Lehrman NJ, Graney JR, Losh S, Jowett EC, Kesler SE (1995) Origin of the McLaughlin mine sheeted vein complex; metal zoning, fluid inclusion, and isotopic evidence. *Econ Geol* 90(8):2156–2181. <https://doi.org/10.2113/gsecongeo.90.8.2156>
- Sherlock RL, Roth T, Spooner ETC, Bray CJ (1999) Origin of the Eskay Creek precious metal-rich volcanogenic massive sulfide deposit, fluid inclusion and stable isotope evidence. *Econ Geol* 94(6):803–824. <https://doi.org/10.2113/gsecongeo.94.6.803>
- Taylor HP (1968) The oxygen isotope geochemistry of igneous rocks. *Contrib Miner Petrol* 19(1):1–71. <https://doi.org/10.1007/bf00371729>
- Taylor HP (1983) Oxygen and hydrogen isotope studies of hydrothermal interactions at submarine and subaerial spreading centers. In: *Hydrothermal Processes at Seafloor Spreading Centers*, 12: 83–139. <https://doi.org/10.1007/bf00371729>
- Taylor HP, Bruno T, Aldo C (1984) $^{18}\text{O}/^{16}\text{O}$ and chemical relationships in K-rich volcanic rocks from Australia, East Africa, Antarctica, and San Venanzo-Cuparello, Italy. *Earth Planet Sci Lett* 69(2):263–276
- Wang RC, Shen WZ, Xu XJ, Lu JJ, Chen XM, Luo YN, Cao ZM (1995) Isotopic geology of the Dashuigou tellurium deposit in Sichuan province, China. *J Nanjing Univ (Natural Sciences)* 31(4):617–624 (in Chinese with English abstract).
- Wang RC, Chen XM, Xu SJ (1996) Complex exsolution of tellurium minerals in the Dashuigou tellurium deposit. *Sci Bull* 41(10):920–922.

- Wang RC, Lu JJ, Chen XM (2000) Genesis of the Dashuigou tellurium deposit in Sichuan province, China. Bull Mineral Petrol Geochem 4:348–349 (**in Chinese with English abstract**).
- Wei JX, Mao JW (1998) Characteristics of ore-forming fluids and their mantle-derived properties in the Dashuigou tellurium deposit. Deposit Geol 17:1091–1094 (**in Chinese with English abstract**).
- Xu Z, Li J (1987) Geological characteristics and mineralization law of the serpentine-asbestos mine in Shimian county of Sichuan province, China. China National Geological Archives (**in Chinese**). <https://doi.org/10.35080/n01.c.73625>
- Xu ZQ, Hou LW, Wang ZX, Fu XF, Huang MH (1992) The orogenic process of the Songpan-Ganzi orogenic belt in China. Geological Publishing House, Beijing (**in Chinese with English abstract**).
- Xu SJ, Shen WZ, Wang RC (1998) Zircon-U-Pb dating of ore-bearing amphibolites from the Dashuigou tellurium deposit. Sci Bull 43(8):883–885.
- Xu YF, Ni P, Wang GG, Pan JY, Guan SJ, Chen H, Ding JY, Li L (2016) Geology, fluid inclusion and stable isotope study of the Huangshan orogenic gold deposit: implications for future exploration along the Jiangshan-Shaoxing fault zone, South China. J Geochem Explor 171:37–54. <https://doi.org/10.1016/j.gexplo.2016.02.004>
- Yichang Institute of Geology and Minerals (1982) Sampling criteria of isotope geology. Geological Publishing House, Beijing (**in Chinese with English abstract**).
- Yin JZ, Shi HY (2019) Nano effect mineralization of rare elements—taking the Dashuigou tellurium deposit, Tibet Plateau, Southwest China as the example. Academia J Sci Res 7(11):635–642. <https://doi.org/10.15413/ajsr.2019.0902>
- Yin JZ, Shi HY (2020) Mineralogy and stable isotopes of tetradymite from the Dashuigou tellurium deposit, Tibet Plateau, southwest China. Sci Reports 10:4634. <https://doi.org/10.1038/s41598-020-61581-3>
- Yin JZ, Shi HY (2021) Fluid inclusions and metallogenetic conditions of the Dashuigou tellurium deposit, Tibet Plateau, Southwest China. Geol Earth Marine Sci 3(3):1–15. <https://doi.org/10.31038/GEMS.2021331>
- Yin JZ, Chen YC, Zhou JX (1994a) Mineralogical research of the Dashuigou independent tellurium deposit in Sichuan province, China. Bull Mineral Petrol Geochem 3:153–155 (**in Chinese with English abstract**).
- Yin JZ, Zhou JX, Yang BC (1994b) Rock-forming minerals and ore-forming minerals of the Dashuigou tellurium ore deposit unique in the world—A preliminary study. Sci Geol Sinica 3(2):197–210.
- Yin JZ, Zhou JX, Yang BC (1994c) Geological characteristics of the Dashuigou tellurium deposit in Sichuan province, China. Earth Sci Front 1(4):241–243 (**in Chinese with English abstract**).
- Yin JZ, Chen YC, Zhou JX (1995a) The metallogenetic age of the world's first independent tellurium deposit. Chin Sci Bull 40:766–767 (**in Chinese with English abstract**).
- Yin JZ, Chen YC, Zhou JX (1995b) K-Ar isotope evidence for age of the first and only independent tellurium deposit. Chin Sci Bull 40(22):1933–1934.
- Yin JZ, Chen YC, Zhou JX (1995c) Original rock of the host rock of the Dashuigou independent tellurium deposit in Sichuan Province, China. Bull Mineral Petrol Geochem 2:114–115 (**in Chinese with English abstract**).
- Yin JZ, Chen YC, Zhou JX (1995d) Introduction of tellurium resources in the world. J Hebei Coll Geol 18(4):348–354 (**in Chinese with English abstract**).
- Yin JZ, Chen YC, Zhou JX (1996a) Geology and geochemistry of host rocks of the Dashuigou independent tellurium deposit in Sichuan Province, China. J Changchun Univ Earth Sci 26(3):322–326 (**in Chinese with English abstract**).
- Yin JZ, Chen YC, Zhou JX (1996b) Geology and geochemistry of altered rocks of the Dashuigou independent tellurium deposit in Sichuan province, China. J Xi'an Coll Geol 18(4):19–25 (**in Chinese with English abstract**).
- Yin JZ, Xiang SP, Chao YH, Yin HY, Shi HY (2022) Petrochemical eigenvalues and diagrams for the identification of metamorphic rocks' protolith, taking the host rocks of Dashuigou tellurium deposit in China as an example. Acta Geochimica. <https://doi.org/10.1007/s11631-022-00583-6>
- Yin JZ (1996a) On the paragenetic model and mineralizing mechanism of the Dashuigou independent tellurium deposit in Shimian County, Sichuan Province, China—the only independent tellurium deposit in the world. Chongqing: Chongqing Publishing House, 190 (**in Chinese with English abstract**).
- Yin JZ (1996b) The paragenetic model and mineralizing mechanism of the Dashuigou independent tellurium deposit in Shimian county, Sichuan - The first and only independent tellurium deposit in the world. Acta Geoscientia Sinica, special issue, 93–97.
- Yu J, Yu F, Qin Z (1989) Relationship between δD and H_2O in some Chinese granites. Chinese Science-Series B 4:433–440 (**in Chinese with English abstract**)
- Zhang QS (1984) Geology and metallogeny of the early precambrian in China. Jilin People's Publishing House, Changchun (**in Chinese with English abstract**).
- Zhang LG (1989) Diagenetic and mineralization theory and ore prospecting. Beijing University of Technology Press, Beijing (**in Chinese with English abstract**).
- Zhang J, Chen YJ, Franco P, Deng J, Chen HY, Wang CM (2013) Geology, C-H-O-S-Pb isotope systematics and geochronology of the Yindongpo gold deposit, Tongbai Mountains, central China: implication for ore genesis. Ore Geol Rev. 53:343–356. <https://doi.org/10.1016/j.oregeorev.2013.01.017>

Springer Nature or its licensor (e.g. a society or other partner) holds exclusive rights to this article under a publishing agreement with the author(s) or other rightsholder(s); author self-archiving of the accepted manuscript version of this article is solely governed by the terms of such publishing agreement and applicable law.